

**$^{63,65}\text{Cu}$  and  $^{17}\text{O}$  spin-echo decay and the static susceptibility  $\chi'(\mathbf{q})$  in  $\text{La}_{1.85}\text{Sr}_{0.15}\text{CuO}_4$** 

R. E. Walstedt and S-W. Cheong

*AT&T Bell Laboratories, 600 Mountain Avenue, Murray Hill, New Jersey 07974*

(Received 7 July 1994)

Data are presented and analyzed for the nuclear spin-echo decay of  $^{63,65}\text{Cu}$  and  $^{17}\text{O}$  in  $\text{La}_{1.85}\text{Sr}_{0.15}\text{CuO}_4$  at  $T=100$  K. The echo-decay data are compared with calculated waveforms in which time fluctuations of coupled neighbor spins are taken into account. Data for the two copper isotopes are found to show the effects of both  $T_1$  and nuclear spin exchange fluctuations. Experimental decay rates for the  $^{63,65}\text{Cu}$  are in good agreement with indirect nuclear spin-spin interactions calculated using values of  $\chi'(\mathbf{q}, 0)$  inferred from neutron-scattering data for  $S(\mathbf{q}, \omega)$  for this system. For  $^{17}\text{O}$ , the echo decay is found to be in good agreement with an interpretation based on Cu-O nuclear dipolar couplings alone, in which the same Cu  $T_1$  and nuclear spin exchange values are employed as for the copper echo decay. Calculated Cu-O indirect couplings of comparable magnitude to the dipole-dipole terms are therefore concluded to be absent. We further conclude that the transferred Cu-O hyperfine coupling is much smaller than that deduced from the measured  $^{17}\text{O}$  NMR shift. It follows that the excitations which provide the  $^{17}\text{O}$  NMR shift and relaxation are separate and distinct from those associated with spin fluctuations on the copper sites. Similar conclusions were reached in a recent study of  $^{17}\text{O}$  nuclear spin-lattice relaxation in this system.

**I. INTRODUCTION**

One of the major unresolved questions concerning spin fluctuation properties of the cuprate superconductors is how to understand the dramatic contrast in nuclear spin-lattice relaxation rate ( $T_1^{-1}$ ) behavior between copper ( $^{63,65}\text{Cu}$ ) and oxygen ( $^{17}\text{O}$ ) sites in the conducting layers.<sup>1,2</sup> These sites lie less than 2 Å from one another, each species surrounded by the opposite, yet for 90 K YBCO ( $\text{YBa}_2\text{Cu}_3\text{O}_7$ ),<sup>3-5</sup> 60 K YBCO ( $\text{YBa}_2\text{Cu}_3\text{O}_{6.5-0.7}$ ),<sup>6-8</sup> and in LSCO ( $\text{La}_{1.85}\text{Sr}_{0.15}\text{CuO}_4$ ),<sup>9-12</sup> the relaxation at the copper site exhibits strong antiferromagnetic enhancement effects, while that at the planar oxygen is at most weakly enhanced with a strikingly different temperature dependence.<sup>2,6</sup> Early on it was pointed out<sup>13,5</sup> that the contrasting hyperfine form factors  $A(\mathbf{q})$  for the copper and oxygen sites could account for the difference in relaxation behavior if one postulated, in a one-band picture, the presence of a sharp antiferromagnetic peak in  $\chi''(\mathbf{q}, \omega)$ , where the relaxation rate is given by

$$(T_1 T)^{-1} = \frac{2\gamma^2 k_B}{g^2 \mu_B^2} \sum_{\mathbf{q}} A(\mathbf{q})^2 [\chi''(\mathbf{q}, \omega)/\omega]_{\omega \rightarrow 0}. \quad (1)$$

Serious efforts have been made along these lines to account for the experimental data using mean-field models of the dynamic susceptibility.<sup>14,15</sup> With an assumed oxygen hyperfine coupling transferred from the two nearest-neighbor copper sites,<sup>13</sup> an antiferromagnetic fluctuation peak would be "invisible" to the oxygen spins, whose relaxation would then be controlled by a flat background term in  $\chi''(\mathbf{q}, \omega)$ . Despite its appealing simplicity, this approach has had difficulty obtaining corroboration from neutron measurements of  $\chi''(\mathbf{q}, \omega)$ . Data for the 60 K

phase of YBCO (Refs. 16, 17) show a peak at  $\mathbf{q} = (\pi, \pi)$  which is marginally narrow enough to give the sharp distinction between sites which is required. Data for the 90 K phase<sup>18,19</sup> give a very wide peak at 40 meV, with spectra at lower energies showing no features resolvable with the available signal-to-noise ratio. Theoretical models<sup>20,21</sup> do not produce the peaks required, with some authors proposing multiple-band effects to account for the YBCO NMR data.<sup>20</sup>

Recent high-quality neutron-scattering results for superconducting LSCO establish this system as an important test case for the foregoing one-band interpretation. Instead of a peak at  $\mathbf{q} = (\pi, \pi)$ , this system has been reported to exhibit four well-resolved incommensurate peaks, with an incommensurability  $\delta$  which is frequency and temperature independent.<sup>22-24</sup> Moreover,  $\delta$  is large enough so that the copper  $T_1$  behavior driven by these peaks leaks over to the oxygen sites as well. One result is a predicted copperlike relaxation behavior for the planar oxygen nuclei which is not observed experimentally.<sup>12</sup> The suggested resolution of this apparent contradiction<sup>12</sup> is that the putative transferred hyperfine coupling to  $^{17}\text{O}$  from the nearby copper sites is much smaller than the total hyperfine coupling measured by the NMR shift. It follows that the  $^{17}\text{O}$  NMR shift and relaxation are dominated by some other agency, i.e., excitations not involving the Cu  $d$  states. This conclusion runs contrary to a large body of theoretical work on single-band models (see, e.g., Refs. 25, 26). In the present paper we seek to further scrutinize the planar  $^{17}\text{O}$  hyperfine interaction by examining the indirect nuclear spin-spin couplings in LSCO which are mediated by an enhanced  $\chi'(\mathbf{q}, 0)$  that is a companion to the  $\chi''(\mathbf{q}, \omega)$  measured by the neutrons. Although  $\chi'(\mathbf{q}, 0)$  is not measured directly, it can be estimated from *absolute* neutron values for  $\chi''(\mathbf{q}, \omega)$  (Refs. 22, 23, 12) by means of the Kramers-Kronig re-

lation. Employing the Pennington-Slichter (PS) formalism for indirect spin-spin coupling,<sup>27</sup> we calculate indirect coupling contributions for the copper lines which dominate the spin-echo decay, as well as a substantial contribution to the <sup>17</sup>O line broadening through an interspecies Cu-O spin-spin coupling term.

In order to measure the foregoing interactions we have investigated the <sup>63,65</sup>Cu and <sup>17</sup>O spin-echo-decay rates. Why this is a useful approach requires some explanation. The traditional means for characterizing echo decay consists<sup>27-29</sup> of dividing out the direct spin-lattice exponential decay and then treating the remaining spin-spin decay effect as an approximately Gaussian process which yields the like-spin second moment of the resonance line. In this "static" approximation, neighbor spins are assumed to be motionless during the decay, i.e., only perturbed by the echo refocusing pulse, which is assumed to be a  $\pi$  pulse. In the present case we found very quickly that this method was inapplicable. For example, we conclude for the planar <sup>17</sup>O that the process is dominated by the unlike Cu-O dipolar coupling, which in the foregoing static picture is completely ineffective. The agency which operates here is spin modulation during the echo decay by copper  $T_1$  and exchange-like flip-flop transitions, for which there is no comprehensive theory. We also found that the copper echo decay did not obey the pulse condition effects or correspondence between isotopes mandated by the static picture. The main obstacle, then, was to find a new way to calculate echo decay in the presence of dynamical effects.

A method for doing such calculations has been developed and is expounded below. It is a straightforward approach in which echo decay is expressed as a statistical average over fluctuation sequences which can be modeled by computer. We present what we believe to be quantitative results for both the copper and oxygen echo-decay curves. Using these methods we have measured the Cu-Cu and Cu-O indirect spin-spin couplings in LSCO. The results have been found to mirror very closely the conclusions in the  $T_1$  study,<sup>12</sup> namely, that the Cu-Cu effect is in agreement with expected behavior, whereas the calculated Cu-O spin-spin interaction is simply found to be absent. The latter result rules out the Cu-O transferred hyperfine coupling as the predominant mechanism of <sup>17</sup>O NMR shift and relaxation. These effects appear, then, to require a separate band not involving the copper orbitals.

The statistical model for calculating echo decay is described and tested on known cases in Sec. II. In Sec. III we present data and analysis of echo-decay results for both the copper and planar oxygen resonance lines in LSCO. A summary and conclusions are given in Sec. IV.

## II. SPIN-ECHO-DECAY ANALYSIS

No comprehensive theory of spin-echo decay in solids has been put forward to date, owing to the inherent complexities of this phenomenon.<sup>30</sup> One usually has resort to a combination of the method of moments for line shape analysis,<sup>30,31</sup> and the invocation of Gaussian and/or Lorentzian line shape function models as a frame-

work for quantitative analyses.<sup>27-29</sup> In the limit of rapid modulation, the density matrix dynamical formulation of motional narrowing can be employed.<sup>30,31</sup> For intermediate cases, the situation is more difficult. In this section we seek to bridge the gap in conventional technique by introducing a method whereby both static and time-varying interactions which generate and condition spin-echo decay are accounted for, leading to quantitative results in a number of cases of interest. This method is especially useful in cases where fluctuation effects hitherto neglected are dominant.

### A. General formulation of echo decay

We develop a formulation of the echo-decay problem which includes interactions between both like and unlike spins and incorporates spin-lattice relaxation effects, i.e., both direct relaxation and spin-lattice modulation of the spin-spin couplings. The nuclear spins observed are the  $\mathbf{I}_i^A$  ( $A$  spins). These are also coupled to the  $\mathbf{I}_k^B$  ( $B$  spins) and to the lattice thermodynamic reservoir by means of hyperfine interactions  $\mathcal{H}_{\text{SL}}^{A,B}$  which we need not specify in detail. The full nuclear spin Hamiltonian may be written

$$\mathcal{H} = \mathcal{H}_Z^A + \mathcal{H}_Z^B + \mathcal{H}_{\text{SS}}^{AA} + \mathcal{H}_{\text{SS}}^{AB} + \mathcal{H}_{\text{SS}}^{BB} + \mathcal{H}_{\text{SL}}^A + \mathcal{H}_{\text{SL}}^B, \quad (2)$$

where the Zeeman terms are  $\mathcal{H}_Z^{A,B} = -\gamma_{A,B}H_0(1 + K_{A,B})\sum_i I_{zi}^{A,B}$ , the spin-spin terms  $\mathcal{H}_{\text{SS}}^{AA}$ , etc., consist of dipolar<sup>30</sup> and indirect coupling<sup>27</sup> contributions, and the spin-lattice terms  $\mathcal{H}_{\text{SL}}^{A,B}$  are considered in general to be anisotropic.

The discussion is greatly simplified by transforming the problem into an interaction representation known as the "rotating frame," i.e., by transforming out the Zeeman terms.<sup>30</sup> Without changing notation, we also eliminate all "nonsecular" spin-spin terms which do not commute with  $\mathcal{H}_Z^A$  and  $\mathcal{H}_Z^B$  and ignore for simplicity the modulating effect of  $\mathcal{H}_Z^{A,B}$  on the spin-lattice terms. The nonsecular terms are always unimportant in the high-field case of interest here. The equation of motion for the rotating frame density matrix  $\rho_R$  is then

$$\frac{d\rho_R}{dt} = -i[(\mathcal{H}_{\text{SS}}^{AA} + \mathcal{H}_{\text{SS}}^{AB} + \mathcal{H}_{\text{SS}}^{BB} + \mathcal{H}_{\text{SL}}^A + \mathcal{H}_{\text{SL}}^B), \rho_R]. \quad (3)$$

The form of the spin-spin coupling terms can be specified in general as<sup>32</sup>

$$\begin{aligned} \mathcal{H}_{\text{SS}}^{AA} &= \mathcal{H}_{zz}^{AA} + \mathcal{H}_{\text{ex}}^{AA} \\ &= \sum_{i>j} \alpha_{ij} I_{zi}^A I_{zj}^A + \sum_{i>j} \delta_{ij} \mathbf{I}_i^A \cdot \mathbf{I}_j^A \end{aligned} \quad (4)$$

in an obvious notation, and

$$\mathcal{H}_{\text{SS}}^{AB} = \mathcal{H}_{zz}^{AB} = \sum_{i,k} \beta_{ij} I_{zi}^A I_{zk}^B. \quad (5)$$

$\mathcal{H}_{\text{SS}}^{BB}$  has the same form as  $\mathcal{H}_{\text{SS}}^{AA}$  [Eq. (4)].

The spin-lattice terms in Eq. (3) have two effects which must be taken account of separately. First, they relax the observed nuclei directly in a process which we take to be statistically independent of any spin-spin relaxation, and thus to act in parallel with the  $T_2$  process.<sup>33–35</sup> Second, they cause the spin-spin terms to fluctuate in time. How we include such fluctuations in the analysis is the topic of Sec. IIB. The Heisenberg terms  $\mathcal{H}_{\text{ex}}^{AA}$  and  $\mathcal{H}_{\text{ex}}^{BB}$  [Eq. (4)] also cause the  $A$ -spin and  $B$ -spin systems, respectively, to fluctuate in time if not inhibited by local inhomogeneities in the Zeeman frequencies. These exchange-like terms do not relax the transverse (echo) magnetization directly, because they commute with  $\sum_i \mathbf{I}_i^A$ . We remind the reader in this connection that the latter terms do not contribute to the second moment in conventional line-broadening theory.<sup>30</sup> These terms will be very important, however, in the analysis below.

The remaining terms in Eq. (2) are  $\mathcal{H}_{zz}^{AA} + \mathcal{H}_{zz}^{AB} + \mathcal{H}_{zz}^{BB}$ .  $\mathcal{H}_{zz}^{BB}$  does not affect the  $A$ -spin echo decay and is therefore dropped. The remaining two terms are the only contributors to the second moment of the  $A$ -spin NMR line and are the primary cause of echo decay in the cases we consider. Since it is not possible to obtain a useful solution directly from Eq. (3), we develop an approximate equation in which all the essential physical effects are included. For this purpose the  $zz$  broadening terms above may be expressed in terms of time-varying local fields  $\Delta h_i(t)$ :

$$\mathcal{H}_{zz}^{AA} + \mathcal{H}_{zz}^{AB} = \gamma_A \sum_i I_{zi}^A \Delta h_i(t), \quad (6)$$

where  $\gamma_A \Delta h_i(t) = \sum_{j(\neq i)} \alpha_{ij} m_j^A(t) + \sum_k \beta_{ik} m_k^B(t)$ . In this expression  $m_j^A(t)$  and  $m_k^B(t)$  are the instantaneous quantum numbers of neighbor spin operators  $I_{zj}^A$  and  $I_{zk}^B$ . Their time variation is a consequence of the spin-spin Heisenberg and spin-lattice coupling terms. The semiclassical representation in Eq. (6) gives the correct second moment contributions from like and unlike spins.<sup>31</sup> In addition to modulating the local fields, spin-lattice terms also produce a direct relaxation effect on transverse spins.<sup>33–35</sup> We include this by inserting a term  $-\rho_R/T_{1E}$  in the equation of motion, which now becomes

$$\frac{d\rho_R}{dt} = -i \left[ \gamma_A \sum_i I_{zi}^A \Delta h_i(t), \rho_R \right] - \frac{\rho_R}{T_{1E}}. \quad (7)$$

$T_{1E}$  is the spin-lattice relaxation time of the spin echo, the derivation of which we discuss in the Appendix.

The solution to Eq. (7) is  $\rho_R(t) = \exp[-i \sum_i I_{zi}^A \Phi_i(0, t)] \rho_R(0) \exp[i \sum_i I_{zi}^A \Phi_i(0, t)] e^{-t/T_{1E}}$ , where

$$\Phi_i(0, t) = \sum_j \alpha_{ij} \int_0^t m_j^A(t') dt' + \sum_k \beta_{ik} \int_0^t m_k^B(t') dt'$$

is the accumulated phase angle for spin  $i$  over the time interval  $(0, t)$ . To develop a formal expression for the spin-echo amplitude, one needs to apply a second excitation pulse (pulse angle =  $\theta_2$ ) at  $t = \tau$  and then evaluate  $M_x(t) = \hbar \gamma_A \text{Tr}[I_x^A \rho_R(t)]$  at  $t > \tau$ ,<sup>36,37</sup> yielding

$$M_x(2\tau)/M_x(0) = \frac{1}{2} (1 - \cos \theta_2) \langle \cos[\Phi_i(0, \tau) - \Phi_i'(\tau_+, 2\tau)] \rangle_i e^{-2\tau/T_{1E}}. \quad (8)$$

In Eq. (8) the average  $\langle \rangle_i$  is over  $A$ -spin sites in the system. The prime on  $\Phi_i'(\tau_+, 2\tau)$  indicates that the  $m_j^A(\tau_+)$  should be modified appropriately to reflect the effects of the  $\theta_2$  pulse. Thus, the  $m_j^A(\tau_+)$  are reversed in sign [ $m_j^A(\tau_+) = -m_j^A(\tau)$ ] or unchanged, with probabilities  $\sin^2(\theta_2/2)$  and  $\cos^2(\theta_2/2)$ , respectively. Using the latter result in Eq. (8) and assuming that the spins are otherwise static, Eq. (8) gives, for small  $\tau$ ,

$$M_x(2\tau)/M_x(0) \approx [1 - 2\tau^2 \sin^2(\theta_2/2) \langle \Delta\omega^2 \rangle_A + \dots] e^{-2\tau/T_{1E}}, \quad (9)$$

where  $\langle \Delta\omega^2 \rangle_A$  is the second moment from  $\mathcal{H}_{zz}^{AA}$  alone [Eq. (4)].<sup>38</sup> This simple result is the basis of much of the echo-decay analysis in the literature.<sup>27–29</sup> For the case of LSCO, however, we find the behavior at variance with Eq. (9). In Sec. IIB, we use Eqs. (7) and (8) as the basis for discussing spin-echo decay in the presence of exchange and  $T_1$ -induced spin flips.

## B. Rate equation model for spin fluctuations

Spin fluctuations are often a key ingredient in the echo-decay process. Considering Eq. (8), we can see that the echo lifetime will be modified if  $m_j^A$  is time varying and, further, that unlike spins make no contribution to the decay rate unless  $m_k^B$  is also time varying. Our source model for dynamics of spin fluctuations consists of the rate equations which govern the  $T_1$  process of individual spins. In this paper we concern ourselves with the fluctuation properties of the ( $I = \frac{3}{2}$ ) <sup>63,65</sup>Cu isotopes in LSCO. Extension to other values of  $I$  is straightforward. In the high- $T$  limit, the magnetic dipole rate equations for the  $m$ -state populations  $p_m$  of a single spin are<sup>39</sup>

$$\begin{aligned} \dot{p}_{3/2} &= -3W_0 p_{3/2} + 3W_0 p_{1/2}, \\ \dot{p}_{1/2} &= 3W_0 p_{3/2} - 7W_0 p_{1/2} + 4W_0 p_{-1/2}, \\ \dot{p}_{-1/2} &= 4W_0 p_{1/2} - 7W_0 p_{-1/2} + 3W_0 p_{-3/2}, \\ \dot{p}_{-3/2} &= 3W_0 p_{-1/2} - 3W_0 p_{-3/2}, \end{aligned} \quad (10)$$

where  $W_0$  is the fundamental transition rate of the  $T_1$  process. In units of  $W_0$  the four characteristic rates of Eq. (10) are 0, 2, 6, and 12. For example, the time constant for decay of the total polarization  $\sum_m m p_m$  is  $T_1 = (2W_0)^{-1}$ . The eigenvectors for the characteristic decay modes are well known.<sup>39,40</sup>

Equations (10) describe the average behavior for a large number of spins, where the  $p_m$ 's can be regarded as probabilities. In order to perform statistical averages such as that in Eq. (8), we require sample fluctuation sequences for individual spins which are stochastic in character. To generate such a sequence we need only one fundamental quantity, namely, the probability  $P_{\text{dwell}}(t)$  that a spin will remain in an  $m$  state for a time  $t$ . Since a spin in any  $m$  state has a uniform probability per unit time of making an outward transition, we clearly have

$P_{\text{dwell}}(t) = e^{-W_{\text{tot}}t}$ , where  $W_{\text{tot}}$  is the total transition rate to neighboring states. From Eq. (10) one has  $W_{\text{tot}} = 3W_0$  for  $m = \pm\frac{3}{2}$  and  $W_{\text{tot}} = 7W_0$  for  $m = \pm\frac{1}{2}$ . A random sequence of dwell times can then be generated by setting  $P_{\text{dwell}}(t)$  equal to a random number on the unit interval,  $R_{0,1}$ . The relation

$$t_{\text{dwell}} = -\ln(R_{0,1})/W_{\text{tot}} \quad (11)$$

is therefore the random fluctuation equivalent of Eq. (10). For  $m = \pm\frac{1}{2}$  we require a second random number to determine which neighboring state the spin in question moves to. With these simple ingredients one can generate fluctuation sequences such as we show in Fig. 1. By averaging over a sufficiently long sample of  $m(t)$ , presumably any function of the  $m_j^{A,B}$  variables can be determined to satisfactory precision.

We illustrate the use of this technique by obtaining, through statistical averaging, curves for the conditional probabilities  $P_{m',m}(t)$  that a spin in state  $m$  at  $t = 0$  will be found in state  $m'$  at time  $t$ . It is a simple matter to calculate these quantities from Eq. (10), where, because of the symmetries  $P_{m',m} = P_{-m',-m}$  and  $P_{m',m} = P_{m,m'}$ , the 16 cases for arbitrary  $(m, m')$  collapse down to 6.<sup>41</sup> Two examples are shown in Fig. 2, where the statistical averages over sequences of  $10^6$  steps are shown as dots, and the calculated decay functions are shown as solid lines. The agreement is very good. By continued averaging, results of high precision can clearly be obtained. In the data analyses below, we use this method to perform the average shown in Eq. (8).

We also test the statistical averaging method with Eq. (8) in the limits of very long and very short  $T_1$ . In the limit of long  $T_1$  one simply has static averaging over random  $m_j^{A,B}$ . One can then check to see, for example, whether the static approximation of Eq. (9) leads to a Gaussian decay with the expected parameters. Four such cases, shown in Fig. 3, illustrate the difference in echo relaxation behavior between <sup>63</sup>Cu and <sup>65</sup>Cu in the planar CuO<sub>2</sub> structure as well as its dependence on pulse

conditions. The data points shown are statistical averages  $\langle \cos[\Phi_i(0, \tau) - \Phi_i(\tau_+, 2\tau)] \rangle_i$  [see Eq. (8)] over  $10^5$  random states of neighbor spins which are given random probabilities of being <sup>63</sup>Cu (probability = 0.69) or <sup>65</sup>Cu (probability = 0.31) at each step. Also shown are calculated decay curves for the <sup>63</sup>Cu (solid lines) and the <sup>65</sup>Cu (dashed lines) for two pulse conditions  $\theta_2 = \pi$  and  $\theta_2 = \pi/2$ . All lines drawn are calculated assuming the decay is given by  $\exp[-2\tau^2 \sin^2(\theta_2/2) \langle \Delta\omega^2 \rangle_A]$ , i.e., a Gaussian particularization of Eq. (9). The data points are seen to exhibit very nearly Gaussian behavior, though with slopes which disagree slightly, but noticeably with the calculated curves. Extensive study has shown that these deviations are not a consequence of incomplete averaging, as they repeat over several independent averages. We find that they are a function of the particular set of neighbor couplings  $\alpha_{ij}$  assumed. The data in Fig. 3 were produced using a set of 30 couplings which vary randomly from zero to some maximum value, with the second moment set near the experimentally measured one for <sup>63</sup>Cu. One supposes that as the number of neighbors increases, the simulated decay curves would, by the central limit theorem, approach the calculated Gaussian forms.

In the short- $T_1$  limit Eq. (8) will give an exponential decay with  $T_2 \gg T_1$ , because of the motional narrowing effect on the spin-spin couplings. This result can be derived in a variety of ways.<sup>30,31</sup> Here, we simply expand  $\langle \cos[ ] \rangle \approx 1 - \frac{1}{2} [ ]^2 + \dots$  [see Eq. (8)] and analyze the squared term, noting that to leading order in the short- $T_1$  limit it takes the form  $-2\tau/T_2$ . It is noteworthy that we consider here primarily the case of unlike spin broadening; otherwise the narrowed  $T_2$  process will be only a minor perturbation on a very short transverse spin-lattice decay process. The central feature in the resulting expression for  $1/T_2$  (Ref. 42) is the autocorrelation function of the  $m_j^B(t)$ , i.e., of the polarization. As mentioned with Eq. (10) above, the relevant autocorrelation function is simply  $e^{-t/T_1}$ . This leads to the simple and intuitive result

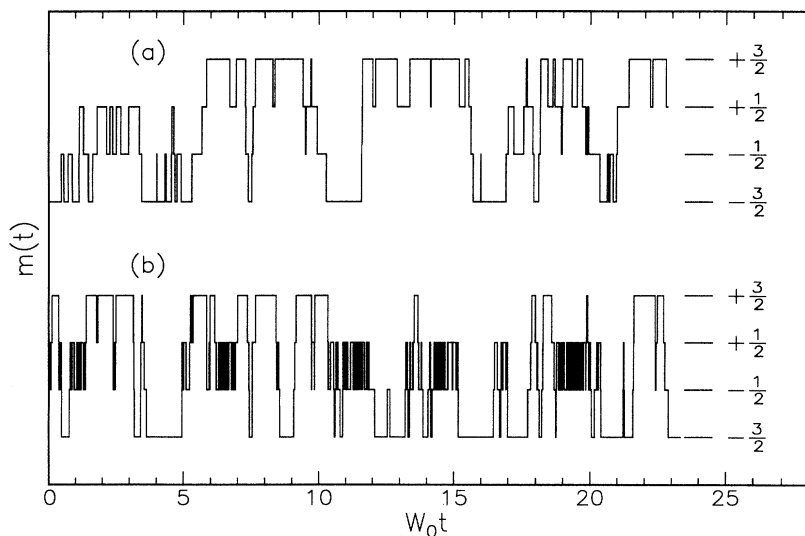


FIG. 1. Sample random fluctuation sequence among the  $m$  states of a spin  $I = \frac{3}{2}$  for (a) normal  $T_1$  transitions only, and (b) for  $T_1$  transitions augmented by modeled exchange fluctuations between the  $\pm\frac{1}{2}$  states at a rate of  $20W_0$ . See text for discussion of random wave forms.

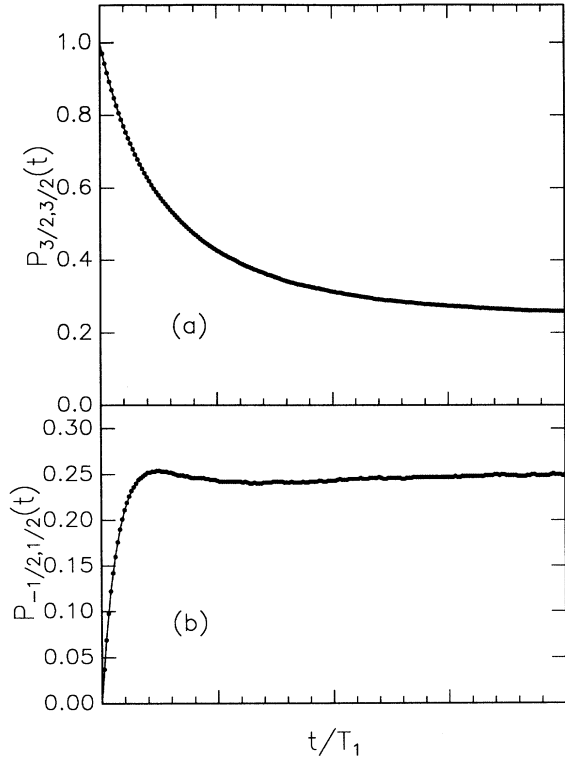


FIG. 2. Plot of (a)  $P_{\frac{3}{2},\frac{3}{2}}(t)$  and (b)  $P_{-\frac{1}{2},\frac{1}{2}}(t)$  wave forms obtained by means of random statistical wave forms (e.g., Fig. 1) (dots) and by solutions of Eq. (10) (Ref. 41) (solid lines). Shown are typical results for averages over  $10^6$ -step sequences.

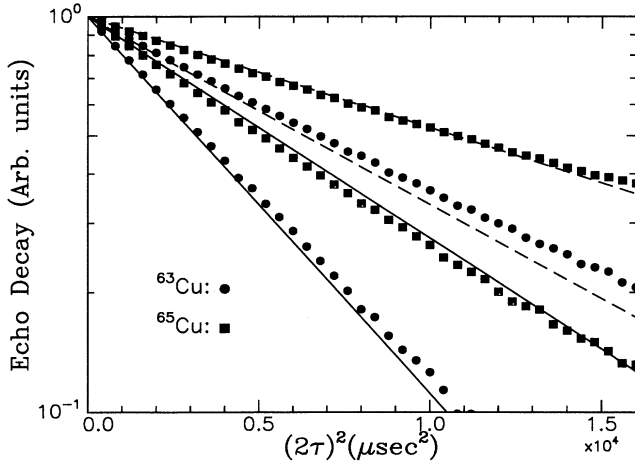


FIG. 3. Calculated spin-echo-decay wave forms for static copper spins in quadratic layer geometry, where the interaction array is 30 neighbors partitioned randomly between  $^{63}\text{Cu}$  (69.1%) and  $^{65}\text{Cu}$  (30.9%) spins, and between  $m = \pm\frac{1}{2}$  (like) and  $m = \pm\frac{3}{2}$  (unlike) spin states. Interactions are selected randomly from 0 to a maximum value, which is adjusted to give second moments close to those found in LSCO. Plotted points show statistical averages obtained from Eq. (8) for  $^{63}\text{Cu}$  (dots) and  $^{65}\text{Cu}$  (squares) for  $\theta_2 = \pi$  and  $\pi/2$ . The solid and dashed lines are Gaussian decay curves based on calculated second moments for  $\theta_2 = \pi$  and  $\pi/2$ , respectively.

$$1/T_{2A} = \langle \Delta\omega^2 \rangle_{AB} T_{1B}. \quad (12)$$

In Fig. 4 echo-decay curves are shown for a series of values of the narrowing parameter  $\langle \Delta\omega^2 \rangle^{\frac{1}{2}} T_{1B}$ . Exponential decay is clearly in evidence for the case  $\langle \Delta\omega^2 \rangle^{\frac{1}{2}} T_{1B} = \frac{1}{4}$ , where a dashed line representing exponential decay with the rate given in Eq. (12) is seen to be in good accord with the statistical average result.<sup>43</sup> As the value of  $T_{1B}$  is lengthened in Fig. 4, the decay time shortens and then executes a minimum as expected.

Finally we consider the application of Eq. (11) to exchange-induced flip-flops between neighboring spins. The rates of such transitions need to be calculated for specific models to see how they would depend on initial and final quantum numbers of the spins involved. The problem is simplified in some sense for LSCO (and many similar materials), because the  $m = \pm\frac{3}{2}$  energy levels of the  $^{63,65}\text{Cu}$  nuclei are broadened to first order by disorder-induced distributions of electric field gradients (EFG's) which interact with the nuclear electric quadrupole moment. Distributions of such energies may be deduced from nuclear-quadrupole-resonance (NQR) spectra,<sup>44,45</sup> which are typically several megahertz wide. In contrast, the  $m = \pm\frac{1}{2}$  levels are only broadened to second order in the quadrupole interaction, resulting in a linewidth which is orders of magnitude smaller. The upshot of this is twofold. First, only spins in the  $\pm\frac{1}{2}$  levels are observed. Second, exchange flip-flops in these systems are only likely to happen for the  $\pm\frac{1}{2}$  levels, and thus there

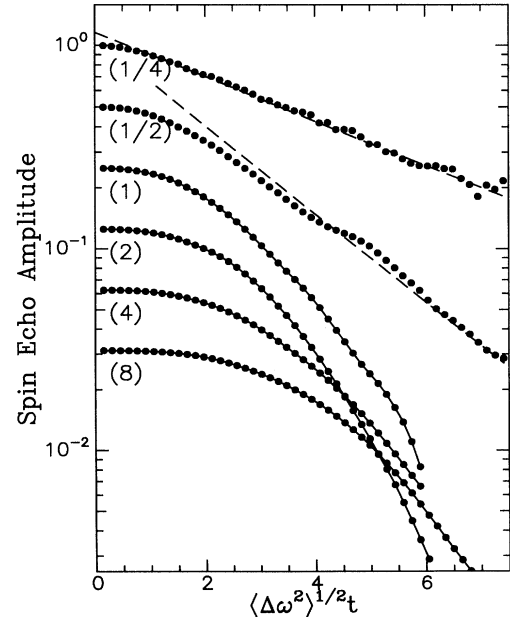


FIG. 4. A series of echo-decay wave forms calculated by means of statistical averages [Eq. (8)] for unlike-spin relaxation through the agency of  $T_1$  fluctuations. Curves for different values of the narrowing parameter  $\langle \Delta\omega^2 \rangle^{1/2} T_1$ , shown in parentheses, are displaced vertically for clarity. For short  $T_1$  values, the curve becomes exponential according to Eq. (12), which is shown as a dashed line for the two top curves. As  $T_1$  increases, the  $e^{-1}$  decay time executes a minimum and then lengthens as the "static" case is approached.

is only one rate constant, which may, however, be widely distributed. We shall model this in practice by augmenting the  $T_1$  rate in Eq. (10) which connects the  $\pm\frac{1}{2}$  levels. As shown in Fig. 1(b), a substantial enhancement of the latter transition rate alters the character of the fluctuations substantially. We discuss the consequences of this effect in connection with the data analysis.

### III. SPIN-ECHO-DECAY RESULTS AND ANALYSIS

In this section we present both copper and oxygen spin-echo-decay data and analyze them with the aid of the techniques developed in Sec. II. Echo-decay data were taken on a partially oriented powder sample of  $\text{La}_{1.85}\text{Sr}_{0.15}\text{CuO}_4$  at  $T = 100$  K, using conventional pulsed NMR methods. The ceramic sample material used, which has been employed in previously reported work,<sup>12</sup> was synthesized using conventional methods.<sup>22</sup> X-ray powder photographs confirmed single-phase purity. Magnetic measurements gave  $T_c = 35$  K. In a slow anneal at  $T = 700$  K approximately 30% of the oxygen was exchanged for  $^{17}\text{O}$ . NMR samples were finely ground, mixed with clear epoxy, and loaded into a Teflon sample container. The specimen so prepared was cured in the NMR probe in a field of 7 T, in order to promote crystalline  $c$ -axis orientation along the field direction.<sup>46</sup> The orientation effect is estimated from the  $^{63}\text{Cu}$  NMR spectrum to be  $\sim 25\%$ . This is enough so that the copper NMR data correspond to essentially fully oriented material. For the  $^{17}\text{O}$  case, however, the second-order quadrupole shifts are negligibly small. Thus, the  $^{17}\text{O}$  data are dominated by the essentially random powder which forms the bulk of the sample.

#### A. $^{63}\text{Cu}$ and $^{65}\text{Cu}$ NMR results and analysis

##### 1. Experimental data

Spin-echo-decay data for both isotopes of copper and a range of pulse conditions are presented in Fig. 5. The curves are displaced vertically for clarity, but are also shown superimposed at the bottom of the figure in order to highlight their similarity. As suggested by Eq. (8), each curve in Fig. 5 has been divided by  $\exp(-2\tau/T_{1E})$ , using the results given in the Appendix to estimate  $T_{1E} = 93 \mu\text{s}$  ( $^{63}\text{Cu}$ ) and  $80 \mu\text{s}$  ( $^{65}\text{Cu}$ ). These are sizable corrections, raising the data points for the longest  $\tau$  values by more than a factor of 3. What remains is decay from spin-spin interaction effects alone. The domination of these decay curves by indirect interactions is clearly established, since dipolar interactions alone would cause a decay on the time scale of Fig. 5 of less than 1%. One notes in these results a remarkably uniform behavior for the two isotopes and for the  $^{63}\text{Cu}$  for pulse conditions with  $\theta_2$  ranging from  $\pi/4$  to  $\pi$  and with two amplitudes of the rf field  $H_1$  differing by a factor of 3. Such behavior stands in sharp contrast with the curves plotted in Fig. 4 for the static approximation, where both the isotopic and

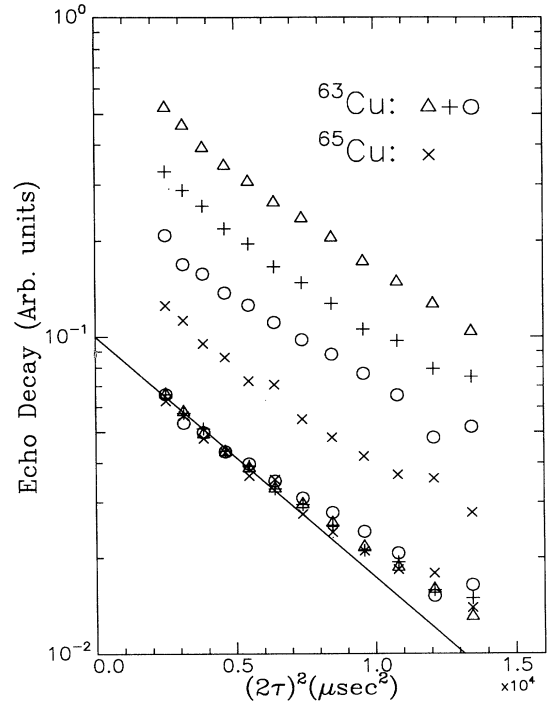


FIG. 5. Measured spin-echo-decay curves for both isotopes of copper in LSCO at  $T = 100$  K, where the curves are displaced vertically for clarity. Refocusing pulse conditions are as follows: Full power,  $\theta_2 \approx \pi$  ( $\Delta$ ). Power down 10 db,  $\theta_2 \approx 3\pi/4$  (+). Power down 10 db,  $\theta_2 \approx \pi/4$  ( $\circ$ ). Full power,  $\theta_2 \approx \pi$  ( $\times$ ). The data plots are superimposed at the bottom to show similarity. The solid line is taken to be the characteristic decay curve to fit.

$\theta_2$  dependences are large. In Fig. 5 we are clearly dealing with a different case where dynamics are important. A second point to note is the upward curvature present in all the curves. Although deviations from strictly Gaussian behavior are to be expected, we suggest that the curvature observed arises either from a distribution of indirect spin-spin coupling strength caused by disorder or from a more slowly relaxing background signal from unoriented sample material. The solid line plotted, given by  $\exp[-(2\tau)^2/T_{2G}^2]$ ,  $T_{2G} = 75.6 \mu\text{s}$ , is taken as a measure of the indirect coupling spin-spin decay time in the analysis below.

##### 2. Indirect coupling between copper nuclei

In order to develop an interpretation of the data in Fig. 5, we estimate the indirect nuclear spin couplings in LSCO using the formulation of this effect given by Pennington and Slichter (PS).<sup>27</sup> The hyperfine coupling at copper site  $\mathbf{r}$  can be written<sup>47,2</sup>

$$\mathcal{H}_{\text{HF}}^{\text{Cu}} = A_c I_z S_z(\mathbf{r}) + A_{ab} [I_x S_x(\mathbf{r}) + I_y S_y(\mathbf{r})] + B \sum_{\hat{r}_{\text{NN}}} \mathbf{I} \cdot \mathbf{S}(\mathbf{r} + \hat{r}_{\text{NN}}), \quad (13)$$

in conventional notation, where  $\mathbf{I}$  and  $\mathbf{S}(\mathbf{r})$  represent the nuclear and electronic spins at site  $\mathbf{r}$ , respectively. The sum on  $\mathbf{r}_{\text{NN}}$  runs over nearest-neighbor unit vectors. In the PS picture, nuclei at sites separated by  $\mathbf{r}_{ij}$  interact

$$\chi_\alpha(\mathbf{r}_{ij}) = \frac{(-1)^{n_x+n_y}}{4\pi^2} \int_{-\pi}^{\pi} dq_x \int_{-\pi}^{\pi} dq_y \cos(q_x n_x) \cos(q_y n_y) \chi'_\alpha(q_x, q_y), \quad (14)$$

where we use the notation  $\mathbf{r}_{ij} = (n_x, n_y)a_L$ ,  $a_L$  being the lattice constant of the  $\text{CuO}_2$  layer, and  $\mathbf{q}$  is in units of  $a_L^{-1}$ . The indirect coupling between a pair of spins separated by  $\mathbf{r}_{ij}$  may then be written  $\mathcal{A}_{ij}^c I_{zi} I_{zj} + \mathcal{A}_{ij}^{ab} (I_{xi} I_{xj} + I_{yi} I_{yj})$ , where

$$\mathcal{A}_{ij}^\alpha = \frac{\gamma_i \gamma_j \hbar}{g_\alpha^2 \mu_B^2} \left[ A_\alpha^2 \chi_\alpha(\mathbf{r}_{ij}) + 2A_\alpha B \sum_{\hat{r}_{\text{NN}}} \chi_\alpha(\mathbf{r}_{ij} + \hat{r}_{\text{NN}}) + B^2 \sum_{\hat{r}_{\text{NN}}} \sum_{\hat{r}'_{\text{NN}}} \chi_\alpha(\mathbf{r}_{ij} + \hat{r}_{\text{NN}} + \hat{r}'_{\text{NN}}) \right]. \quad (15)$$

In this expression the hyperfine constants are in units of gauss/(unit electron spin) and  $\alpha = ab$  or  $c$ . In the prefactor the nuclear gyromagnetic ratios  $\gamma_i$  and  $\gamma_j$  correspond to the isotopes (<sup>63,65</sup>Cu) at those sites. Using Eq. (15), the coefficients in Eq. (4) may be expressed  $\alpha_{ij} = \mathcal{A}_{ij}^c - \mathcal{A}_{ij}^{ab}$  and  $\delta_{ij} = \mathcal{A}_{ij}^{ab}$ . The Cu hyperfine constants in Eq. (15) are estimated from published data:<sup>48</sup> ( $A_{ab}, A_c, B$ )  $\approx$  (4, -277, 72.5) kG/spin.

To evaluate  $\chi_\alpha(\mathbf{r}_{ij})$  [Eq. (14)] and, thus, the indirect coupling coefficients  $\mathcal{A}_{ij}^{ab,c}$  [Eq. (15)], we make use of recent neutron-scattering data to obtain estimates of  $\chi'_\alpha(\mathbf{q}) \equiv \chi'_\alpha(\mathbf{q}, 0)$ . The latter quantity is related to  $\chi''_\alpha(\mathbf{q}, \omega)$  by the Kramers-Kronig relation

$$\chi'_\alpha(\mathbf{q}) = \int_0^\infty d\omega \chi''_\alpha(\mathbf{q}, \omega) / \omega. \quad (16)$$

Measurements of the (effective) powder average  $\chi''(\mathbf{q}, \omega)$  for  $\text{La}_{1.86}\text{Sr}_{0.14}\text{CuO}_4$  with absolute amplitude calibration have now been reported<sup>23</sup> for energies up to 15 meV and temperatures ranging from 4.2 K to 300 K.<sup>49</sup> These data have been fitted to the form

$$\chi''(\mathbf{q}, \omega) = \frac{\chi_0''(\omega, T) \kappa^4(\omega, T)}{[\kappa^2(\omega, T) + R(\mathbf{q})]^2}, \quad (17)$$

where  $\kappa^2(\omega, T) = \kappa_0^2 + a_L^{-2} [(k_B T / E_T)^2 + (\hbar\omega / E_\omega)^2]$  is an inverse squared length scale which determines the widths of the peaks in  $\mathbf{q}$  space and  $R(\mathbf{q}) = \frac{1}{8\pi^2 a_L^2 \delta^2} \{ [(q_x - q_y)^2 - \delta^2 \pi^2]^2 + [(q_x + q_y)^2 - \delta^2 \pi^2]^2 \}$ , where the  $q_\alpha$  are in units of  $a_L^{-1}$  and the origin of  $\mathbf{q}$  is at  $(\pi, \pi)$ . In  $R(\mathbf{q})$  and  $\kappa$ ,  $a_L$  ( $= 3.8 \text{ \AA}$ ) is the lattice constant and  $\delta = 0.245$  is the temperature- and energy-independent incommensurability parameter. Fitting Eq. (17) to neutron data yields  $\kappa_0 = 0.034 \text{ \AA}^{-1}$  and  $E_T = E_\omega = 47 \text{ meV}$ .<sup>23</sup>

Since the data given for the peak amplitude  $\chi_0''(\omega, T)$  (Ref. 23) cover an insufficient energy range to complete the integral in Eq. (16), we carry out an approximate evaluation based on the following assumptions: (1)  $\chi_0''(\omega, T)$ , which varies linearly with  $\omega$  at low energies, is assumed to reach a peak value at an energy  $\omega_{\text{peak}} \propto T$ , after which it remains constant up to some high frequency

via their hyperfine coupling and a transfer susceptibility  $\chi_\alpha(\mathbf{r}_{ij})$  which is defined in terms of the anisotropic, zero-frequency real susceptibility  $\chi'_\alpha(\mathbf{q})$  as follows:

cutoff  $\omega_{\text{CO}}$  and (2), the scaling of  $\kappa(\omega, T)$  given above may be extrapolated to energies of  $\sim 50 \text{ meV}$  or so. The peak in  $\chi_0''(\omega, T)$  was actually observed at  $T = 35 \text{ K}$ , and the ansatz that the position of this peak varies  $\propto T$  is consistent with the general  $\omega/T$  scaling exhibited by these data.<sup>23</sup> From the value  $\omega_{\text{peak}} (T = 35 \text{ K}) \simeq 7 \text{ meV}$ , we estimate  $\omega_{\text{peak}} (T = 100 \text{ K}) = 20 \text{ meV}$ . The variation of  $\chi_0''(\omega, T)/\omega$  for  $T = 100 \text{ K}$  is then modeled as shown in the inset to Fig. 6, where the flat portion is the interpolated initial slope from data in (Ref. 23), the break is at  $\omega_{\text{peak}} (100 \text{ K})$ , and  $\omega_{\text{CO}}$  is used as a variable parameter. With this representation and the foregoing parameter values, we then perform numerical integration with Eqs. (16) and (17) to determine  $\chi'_\alpha(\mathbf{q})$  for arbitrary  $\mathbf{q}$ , and thence to evaluate  $\chi_\alpha(\mathbf{r}_{ij})$  with Eq. (14).

The indirect Cu spin-spin couplings derived from the foregoing scheme extend over a sizable region of the sur-

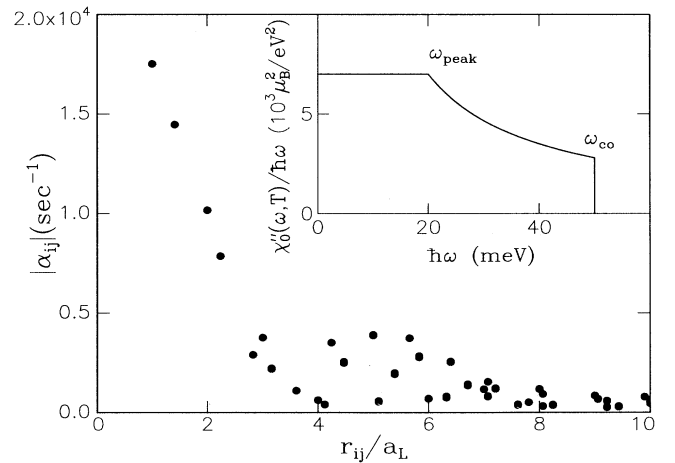


FIG. 6. Distribution of indirect <sup>63</sup>Cu-<sup>63</sup>Cu  $c$ -axis coupling constants calculated from the nominal parametrization for  $\chi'(\mathbf{q})$  stated in the text [Eqs. (16),(17)] (dots). Points shown are absolute values greater than 2% of the maximum occurring in one quadrant of the plane. Inset: Energy dependence of powder average  $\chi_0''(\omega, T)$  [Eq. (17)] modeled using the results of Ref. 23 as described in the text.

rounding lattice as shown in Fig. 6, where we plot absolute values  $|\alpha_{ij}|$  vs  $r_{ij}$  for one quadrant of the lattice, including only values greater than 2% of the maximum. For echo decay the critical parameter is the second moment.<sup>38</sup> The value of this quantity derived from the calculations described is in good agreement with our experimental data (see next subsection for details). Because of the arbitrariness of the model energy profile (Fig. 6, inset), we conclude only that the neutron data are consistent with the  $^{63,65}\text{Cu}$  echo-decay results under reasonable assumptions about the unknown portion of the energy dependence of  $\chi''(\mathbf{q}, \omega)$ . More importantly, the indirect coupling calculation scheme serves as a basis for determining the relative strengths of this effect for Cu-Cu coupling and Cu-O coupling, as discussed in Sec. III B.

### 3. Data analysis and discussion

Using Eq. (8) and the statistical averaging technique described in Sec. II, we have evaluated the expected echo-decay curves for both isotopes of copper, using various assumptions about the dynamical behavior, in an effort to determine what combination of circumstances leads to the observed behavior in Fig. 5. The calculations were carried out with 30 neighbors to each spin  $i$  in Eqs. (4) and (5), where the coupling coefficients  $\alpha_{ij}$  were taken to vary randomly between zero and some maximum value as an approximate representation of the distribution in Fig. 6. The scale of the  $\alpha_{ij}$  distribution is adjusted to give the approximate slope of the  $^{63}\text{Cu}$  echo decay. Note that the signs of the  $\alpha_{ij}$  are immaterial in the high-temperature approximation. For reference purposes, the calculated static decay curves for both  $^{63}\text{Cu}$  and  $^{65}\text{Cu}$  are shown in both panels of Fig. 7 with solid lines drawn through them.

The introduction of dynamics is done in two steps. First, in Fig. 7(a), we introduce normal  $T_1$  fluctuations among the neighbors during the decay. This shortens the decay time for both isotopes, the effect being fractionally greater for the  $^{65}\text{Cu}$ . To understand this differential effect, we note that for either isotope the neighbor spins are divided into like spins (the same isotope with  $m = \pm\frac{1}{2}$ ) and unlike spins (all others). The like-spin decay contribution is weakened by  $T_1$  fluctuations, whereas the unlike spins only contribute when  $T_1$  fluctuations are introduced. The  $^{65}\text{Cu}$  have roughly twice the ratio of unlike- to like-spin neighbors as the  $^{63}\text{Cu}$ , explaining their greater broadening effect with  $T_1$ .

In Fig. 7(b) exchange fluctuations are introduced between the  $\pm\frac{1}{2}$  levels of the neighbor spins in addition to the  $T_1$  transitions. The exchange fluctuation rate between the  $\pm\frac{1}{2}$  levels is set at  $(50 \mu\text{s})^{-1}$ , which is slightly larger than  $\langle A_{ij}^{ab} \rangle_{\text{rms}}$  [Eq. (15)]. For reasons noted above this has a greater weakening effect on the  $^{63}\text{Cu}$  decay. Curiously, there is almost no effect on the  $^{65}\text{Cu}$ .<sup>52</sup> The net result is that decay curves for the two isotopes are brought into near coincidence, as is observed experimentally. We argue from this result that exchange dynamics must be operating between the  $m = \pm\frac{1}{2}$  levels in LSCO

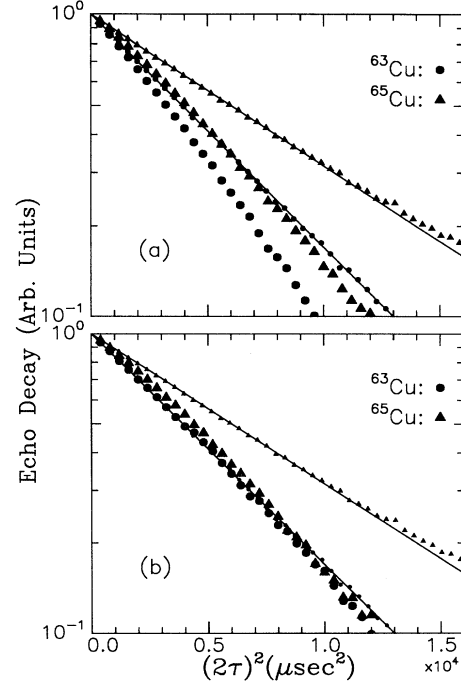


FIG. 7. Echo-decay curves for  $^{63}\text{Cu}$  (large dots) and  $^{65}\text{Cu}$  (large triangles) calculated by statistical average [Eq. (8)] in the presence of (a)  $T_1$  fluctuations (only) among the neighbor spins and (b) both  $T_1$  and exchange fluctuations, with the latter taking place between the  $\pm\frac{1}{2}$  levels at a rate of  $(50 \mu\text{s})^{-1}$ . Shown for reference in both panels are static decay curves for both isotopes with solid lines passed through them, the  $^{63}\text{Cu}$  curve being adjusted to coincide with the solid line through the data in Fig. 5.

in order for the decay time to be nearly identical for the two copper isotopes. Exchange fluctuations also tend to wash out the dependence of the decay time on pulse angle. Thus, their presence would explain the extremely weak dependence on  $\theta_2$  observed in Fig. 5.

The results in Fig. 7 enable us to extract  $\langle \Delta\omega^2 \rangle_A$  for  $^{63}\text{Cu}$  (Ref. 38) from the measured slope in Fig. 5 (solid line),  $1/T_{2G}^2 = 1.74 \times 10^8 \text{ s}^{-2}$  ( $T_{2G} = 76 \mu\text{s}$ ). Thus,  $\langle \Delta\omega^2 \rangle_A = 2f_{\text{corr}}/T_{2G}^2$ , where from Fig. 7 the correction factor  $f_{\text{corr}} \simeq 0.9$ . This gives  $\langle \Delta\omega^2 \rangle_A = 3.1 \times 10^8 \text{ s}^{-2}$ , which yields in turn  $\sum_j \alpha_{ij}^2 = 3.6 \times 10^9 \text{ s}^{-2}$ . Calculating the  $\alpha_{ij}$  using Eq. (15) and the results of the previous subsection, we find a quantitative correspondence with  $\omega_{\text{CO}} \sim 46 \text{ meV}$  as shown in the inset to Fig. 6. Again, we note that the arbitrariness of the shape assumed for  $\chi_0''(\omega, T)$  renders the details of this finding only qualitatively correct. Nonetheless, it is important to note that the portion of  $\chi_0''(\omega, T)$  beyond  $\omega = \omega_{\text{peak}}$  gives more than half of the calculated weight of  $\chi_\alpha(\mathbf{r}_{ij})$ . The high-frequency behavior of  $\chi''(\mathbf{q}, \omega)$  is therefore quite narrowly circumscribed by the measured spin-spin coupling strength.

## B. $^{17}\text{O}$ Spin-echo-decay and analysis

### 1. Experimental data

The  $^{17}\text{O}$  spin-echo-decay data at  $T = 100$  K are plotted semilogarithmically against  $(2\tau)^2$  in Fig. 8. This curve was measured at the center of the  $(-\frac{1}{2} \leftrightarrow \frac{1}{2})$  transition peak<sup>12</sup> with the field along the  $c$  axis of the partially oriented sample. Nonetheless, the signal is strongly dominated by the contribution from unoriented crystallites. The decay is seen to consist of a rapid decline followed by a much flatter decrease, the latter corresponding to  $\sim 30\%$  of the signal amplitude. As we shall see in detail below, the  $^{17}\text{O}$  echo decay is dominated by dipolar coupling with the two nearest-neighbor copper sites, which lie only 1.9 Å away from the oxygen. This unlike-spin coupling term is effective, because it is modulated by copper  $T_1$  fluctuations which are relatively fast on the time scale of Fig. 8. The slowly relaxing portion of the echo decay is attributable to the  $(1 - 3\cos^2\theta)$  angular variation of the dipolar coupling, where  $\theta$  is the angle between the field direction and the Cu-O bond axis. Near  $\theta = 55^\circ$  in a powder average there occurs a substantial number of weakly coupled spins which produce a slowly decaying echo component. The behavior of these weakly coupled spins provides a sensitive test for the presence of the more nearly isotropic indirect coupling.

### 2. Dipolar vs indirect coupling with the planar $^{17}\text{O}$ sites

We now proceed to calculate both the dipolar and indirect couplings involving the planar  $^{17}\text{O}$  nuclei and to establish a hierarchy of relative importance. Of the purely dipolar terms, the two nearest-neighbor  $^{63,65}\text{Cu}$  sites give a powder average second moment  $\langle\Delta\omega^2\rangle_{AB}^{\text{dip}} = 6.25 \times 10^6 \text{ s}^{-2}$ , where in the notation of Sec. II we now consider  $^{17}\text{O}$  to be the  $A$  spins and the  $B$  spins to be both isotopes of copper. The remainder of the copper sites only make a further 2% contribution to  $\langle\Delta\omega^2\rangle_{AB}^{\text{dip}}$ ; their dipolar contribution is henceforth neglected. The  $^{17}\text{O}$ - $^{17}\text{O}$  "like-spin" dipolar broadening effect is weakened by the  $\approx 30\%$  isotopic abundance and by another factor of  $\sim 3$ , which arises because only spins with  $m = \pm\frac{1}{2}$  contribute to the second moment  $\langle\Delta\omega^2\rangle_{AA}$ . The result is  $\langle\Delta\omega^2\rangle_{AA} < 0.02\langle\Delta\omega^2\rangle_{AB}^{\text{dip}}$ . The  $A$ - $A$  dipolar couplings are therefore negligible as well.

Considering next the indirect couplings, we take for the planar  $^{17}\text{O}$  hyperfine interaction,<sup>13-15,53-55</sup>

$$\mathcal{H}_{\text{HF}}^{\text{O}} = \sum_{\alpha=x,y,z} C_{\alpha} I_{k\alpha}^A [S_{\alpha}(\mathbf{r}_k - \hat{r}_{\text{NN}}/2) + S_{\alpha}(\mathbf{r}_k + \hat{r}_{\text{NN}}/2)] \quad (18)$$

$$\beta_{ik}^{\alpha} = \frac{\gamma_{17}\gamma_{\text{Cu}}\hbar}{g_{\alpha}\mu_B^2} \left\{ C_{\alpha} A_{\alpha} [\chi_{\alpha}(\mathbf{r}_{ik} + \hat{r}_{\text{NN}}/2) + \chi_{\alpha}(\mathbf{r}_{ik} - \hat{r}_{\text{NN}}/2)] + BC_{\alpha} \sum_{\hat{r}'_{\text{NN}}} \left[ \chi_{\alpha}(\mathbf{r}_{ik} + \hat{r}'_{\text{NN}} + \hat{r}_{\text{NN}}/2) + \chi_{\alpha}(\mathbf{r}_{ik} + \hat{r}'_{\text{NN}} - \hat{r}_{\text{NN}}/2) \right] \right\}, \quad (19)$$

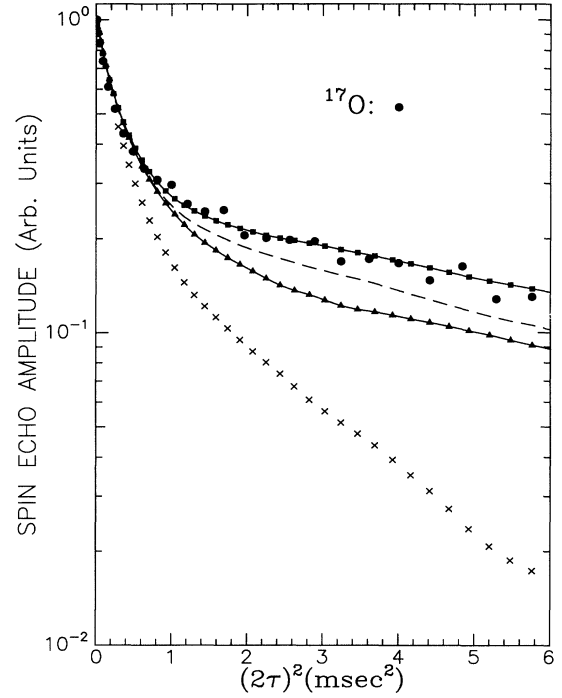


FIG. 8. Spin-echo-decay data for  $^{17}\text{O}$  (dots) are plotted semilogarithmically against  $(2\tau)^2$ , along with several calculated curves. With nearest-neighbor dipolar couplings only, the solid curve with triangles was calculated using Eq. (8) with  $T_1$  transitions (only) among copper neighbors, averaging the quantization axis over the unit sphere. The solid curve with squares was calculated similarly, with both  $T_1$  and exchange transitions and with anisotropies as described in the text. Indirect coupling between Cu and O, with  $\chi_{\alpha}(\mathbf{q})$  scaled to the value required in the copper case, is shown combined with the dipolar coupling with both  $T_1$  and exchange transitions ( $\times$ ) as described above. As a further comparison, we show a calculated curve for the case of dipolar couplings combined with indirect couplings scaled to have a second moment [i.e.,  $\sum_k \beta_{ik}^2$ ; see Eq. (4)] which is a factor of 10 smaller than that obtained from Eq. (19) (dashed line). In each case the effect of anisotropic  $T_{1E}$  is included as formulated in the Appendix.

in the notation of Eq. (13), where  $\mathbf{r}_k$  is the location of the  $^{17}\text{O}$  site and  $\pm\hat{r}_{\text{NN}}/2$  gives the displacement to the nearest-neighbor copper sites. The  $^{17}\text{O}$ - $^{63,65}\text{Cu}$  indirect coupling resulting from Eq. (18) is substantial, however, and has the form of  $\mathcal{H}_{AB}^{zz}$  [Eq. (5)], with

$\alpha = a, b, c$ , where now all directions come into play, because we consider arbitrary field (i.e.,  $z$ -axis) orientation. The  $\chi_\alpha(\mathbf{r})$  values in Eq. (19) are taken from calculations presented in Sec. III A to interpret the  $^{63,65}\text{Cu}$  echo decay. For a field direction given by Euler angles  $(\theta, \phi)$ , the effective coupling coefficient is  $\beta_{ik}^a \sin^2 \theta \cos^2 \phi + \beta_{ik}^b \sin^2 \theta \cos^2 \phi + \beta_{ik}^c \cos^2 \theta$ . Using the planar oxygen hyperfine constants (see the Appendix) and anisotropic  $g$  tensor from Ref. 12, we find that Eq. (19) leads to second-moment values  $\langle \Delta\omega^2 \rangle_{AB} = (0.28, 0.48, 1.58) \times 10^7 \text{ s}^{-2}$  with the field in the  $(a, b, c)$  direction, respectively. With sufficient  $T_1$  modulation, these values are clearly large enough to cause observable echo-decay effects.

There is also indirect  $^{17}\text{O}$ - $^{17}\text{O}$  coupling which results when the hyperfine terms in Eq. (18) are employed twice in the PS formalism. Estimates of the second-moment contribution generated by this coupling show a rather weak decay process, in which the echo amplitude relaxes by only  $\sim 5\%$  across the time span of Fig. 5. We omit any further discussion of this term.

### 3. Analysis and discussion

The  $^{17}\text{O}$  echo decay has been analyzed using the statistical averaging method with Eq. (8) as described above. The ingredients of this process are the interactions spelled out in the previous subsection, an anisotropic copper  $T_1$  process, and an anisotropic exchange fluctuation process among the copper neighbor spins similar to those employed for the copper case. The net result of these efforts is the conclusion that it is only possible to achieve good agreement with the observed results with the dipolar interaction *alone*, and that it is also necessary to include an anisotropic spin-spin exchange fluctuation process consistent with the calculated indirect Cu-Cu couplings from Sec. III A 2. The latter finding is in agreement with the copper spin-echo results discussed earlier. We first discuss the dipolar coupling analysis and then comment on the effect of the calculated indirect Cu-O interactions.

Calculated echo-decay curves to be compared with the data of Fig. 8 were obtained by averaging Eq. (8) over the unit sphere, including the anisotropic  $T_{1E}$  for  $^{17}\text{O}$  discussed in the Appendix. The oriented portion of the sample seemed to contribute very little to the observed signal, possibly due to shift anisotropy. The dipolar terms were limited to only the two nearest neighbors in what is expected to be an excellent approximation (see the previous subsection). These terms both vary as  $(3 \cos^2 \theta_a - 1)$ , where  $\theta_a$  is the angle the quantization axis makes with the  $a$  direction (i.e., the Cu-O bond axis) in the crystal lattice. Using Cu  $T_1$  anisotropy data from the literature,<sup>56</sup> we obtain a good fit to the data using  $T_1 = T_{1c}/(1 + 1.6 \sin^2 \theta_c)$ , where  $T_{1c} = 0.54 \text{ ms}$  is the NQR value at  $T = 100 \text{ K}$ .<sup>12</sup> In Fig. 8 the solid triangles show the curve which results when the dipolar fields are assumed to be modulated by  $T_1$  fluctuations alone. There is no adjustable parameter whereby we could improve the fit shown.

On the other hand, a quantitative fit to these data is obtained if we introduce spin-spin exchange fluctuations between the  $\pm \frac{1}{2}$  states of the copper spins. Such fluctuations are driven by the  $\delta_{ij}$  terms [Eq. (4)], which have been calculated as described in Sec. III A 2. The relative magnitudes of  $\mathcal{A}_{ij}^{ab}$  and  $\mathcal{A}_{ij}^c$  [Eq. (15)] for Cu-Cu coupling are such that  $\delta_{ij}$  will increase by a factor  $\sim 4$  between the  $c$ -axis and  $ab$ -plane field orientations. The exchange flip rate has been set to  $\simeq (50 \mu\text{s})^{-1}$  for the  $c$ -axis case, as was done above in Sec. III A 3. In accord with the expected anisotropy [Eq. (15)], the flip rate was set to vary as  $(1 + 3 \sin^2 \theta_c)$ , where  $\theta_c$  is the field angle with the  $c$  axis. The curve obtained with these conditions is shown as squares with a solid line through them, and is seen to be in very good agreement with the echo data. A 25% variation in either the  $T_1$  anisotropy or the exchange flip rate with its anisotropy results in a noticeable deviation from the data.

To examine the effect of the calculated indirect Cu-O coupling on  $^{17}\text{O}$  echo decay, these couplings have been assumed to be distributed over the ten nearest-neighbor copper spins, with their magnitudes adjusted to give the calculated anisotropic second moment. The dipolar couplings remain, of course, unchanged. Decay curves have been calculated using Eq. (19) and plotted in Fig. 8 assuming only the case of  $T_1$  plus exchange flips ( $\times$ ). The resulting curve is strongly at variance with the experiment. In order to help quantify the discrepancy between the calculated indirect coupling and the observed  $^{17}\text{O}$  echo decay, we also plot in Fig. 8 a calculated decay curve corresponding to indirect coupling with a second moment which is 10% of the value calculated as described above (dashed line). The result is a decay curve which is still noticeably steeper than the experimental data. We conclude that any indirect Cu-O coupling which is present is smaller in amplitude by at least a factor of 3 than the values calculated in Sec. III B 2.

## IV. SUMMARY AND CONCLUSIONS

We have sought to examine the hyperfine couplings in LSCO through measurements of indirect spin-spin coupling as formulated in Ref. 27. Choosing spin-echo decay as the technique for evaluating spin-spin couplings, we have also presented a method for calculating spin-echo-decay wave forms using computer simulation of random spin fluctuation sequences. This stochastic method has been used to perform simultaneous averages over sets of  $N$  neighbor spins of an echo-decay function, as a function of the time  $\tau$  separating spin-echo excitation and refocusing pulses, using values of  $N$  up to 30. This method allows the practitioner to move beyond the traditional static Gaussian approximation to perform quantitative spin-echo-decay analysis of cases where motion of the spins is an important factor. On the other hand, in the static limit, this technique finds the expected Gaussian behavior with decay times in reasonable agreement with earlier calculations.

The foregoing technique has been applied to the cases of  $^{63,65}\text{Cu}$  and planar  $^{17}\text{O}$  spin-echo decay in LSCO.

For the copper isotopes, echo decay is dominated by indirect spin-spin coupling mediated by an enhanced  $\chi'(\mathbf{q})$  which is closely related to the multiply peaked  $\chi''(\mathbf{q}, \omega)$  which has been very thoroughly characterized by neutron-scattering studies.<sup>22-24</sup> The echo-decay calculations succeed in explaining anomalous features of the copper data, namely, that the decay curves for the two isotopes are nearly identical and are essentially independent of refocusing pulse characteristics. The echo analysis also gives a measure of the indirect Cu-Cu spin-spin couplings which corresponds to a reasonable upper frequency limit for  $\chi''(\mathbf{q}, \omega)$  in the Kramers-Kronig estimate of  $\chi'(\mathbf{q})$ . These results support a recent analysis of the low-temperature <sup>63</sup>Cu  $T_1$  process in LSCO based on the same body of neutron data.<sup>12</sup> It is important to note, however, that recent neutron results at higher temperatures show that the incommensurate susceptibility peaks dominate the copper  $T_1$  process only below  $\sim 100$  K, their contribution being completely swamped by some other, unknown contribution by room temperature.<sup>23</sup>

One surprise finding is that of the importance of spin-spin exchange flip processes in achieving quantitative agreement with both the <sup>63,65</sup>Cu and <sup>17</sup>O echo-decay data. These have been assumed to be absent, i.e., inhibited by local inhomogeneities, by many workers.<sup>27-29,35</sup> The crucial observations here are the comparison of the copper isotopes and the absence of significant pulse and power dependence. The latter effects make no sense whatever if the spins are completely static. It is especially surprising to find mutual spin flips active in LSCO, where there is a great deal of local inhomogeneity induced by Sr doping. Thus, it is all the more likely that they are also present in undoped LaCuO<sub>4</sub> and stoichiometric YBa<sub>2</sub>Cu<sub>3</sub>O<sub>7</sub>.

The spin-echo-decay analysis of Sec. II also gives a quantitative interpretation of the <sup>17</sup>O spin-echo-decay data for  $T = 100$  K, with, however, only Cu-O nearest-neighbor dipolar couplings required. These are modulated by  $T_1$  and exchange as was the case for copper. Inclusion of the indirect Cu-O couplings given by the PS formulas leads to striking disagreement with the experimental data. The situation here mirrors that of spin-lattice relaxation in LSCO.<sup>12</sup> That is, the relaxation time estimated for the copper based on neutron values of  $\chi(\mathbf{q}, \omega)$  is in good accord with measured values, while the corresponding  $T_1$  process for the planar oxygen is simply not observed. Among the possible explanations for this, we suggest the most likely to be that the transferred Cu-O hyperfine interaction [Eq. (18)] is much smaller than that estimated from the NMR shift and susceptibility. The calculations presented in Fig. 8 suggest that the discrepancy is at least a factor of 3. It follows from this that the dominant NMR shift and relaxation effects for the planar oxygen spins come from a carrier band not coupled to the copper orbitals. It is therefore not possible to account for these results within the widely discussed one-band models for the cuprate superconductors.

Alternative explanations for the oxygen results have been stated in Ref. 12. These are, first, that  $\chi(\mathbf{q}, \omega)$  might be frequency dependent in such a way that the incommensurability  $\delta$  disappears at NMR frequencies. To

this we can only suggest that at a few meV of energy one is already in the low-frequency asymptotic regime, where  $\delta$  is frequency independent. Lower-frequency neutron data would be very helpful in resolving this point. Another possibility is that there are domains in the magnetic short-range order in LSCO, with disclinations which render a commensurate peak in  $\chi''(\mathbf{q}, \omega)$  into four separate maxima. This point of view has been expounded in a recent paper.<sup>57</sup> We only note that the incommensurability is very reasonably accounted for by Fermi surface nesting effects, including its dependence on doping.<sup>21,22</sup>

Finally, we comment on some of the possible consequences of there being an "oxygen" band in this system. We know from the  $T_1$  behavior of both <sup>63</sup>Cu and planar <sup>17</sup>O (Ref. 12) that there is a second *term* in the dynamic susceptibility. If this term belongs to an oxygen band, then the measured shifts and susceptibilities must be partitioned between two bands. The hyperfine constants for LSCO may then vary from those we have used here.<sup>48</sup> Based on the latter values, the anisotropy of the copper  $T_1$  is estimated to be much larger than the measured value  $T_{1c}/T_{1ab} = 2.6$ .<sup>56</sup> The presence of a significant contribution to the Cu  $T_1$  from an oxygen band could explain both the observed anisotropy and the unusual temperature dependence of the Cu  $T_1$ .<sup>23</sup>

## ACKNOWLEDGMENTS

It is a pleasure to acknowledge substantive discussions with G. Aeppli, P. Littlewood, A. Millis, and B. S. Shastri.

## APPENDIX

We discuss the effect of spin-lattice relaxation on spin echoes in solids, and derive the numbers quoted in the text. Spin-lattice relaxation of a spin echo excited from ( $m \leftrightarrow m+1$ ) transitions of a nucleus of spin  $I$  is in general different from the usual magnetization recovery  $T_1$  process. The echo-decay time constants can be calculated using the dynamical equation of motion for the density matrix.<sup>30,31</sup> A number of special case results have been given in the literature.<sup>33-35</sup> Here we state a general result pertaining to the ( $\frac{1}{2} \leftrightarrow -\frac{1}{2}$ ) transition for an arbitrary odd half integer spin quantum number  $I$  in a lattice having three inequivalent axes. The behaviors of <sup>63,65</sup>Cu and <sup>17</sup>O nuclei in LSCO as discussed in this paper are cases in point.

In an isotropic system we write  $T_1^{-1} = 2W_0$ , where the rate of spin-lattice transitions between states  $m$  and  $m+1$  for an individual spin is written<sup>31</sup>  $W_{m+1,m} = (I-m)(I+m+1)W_0$ . In an anisotropic system we associate rate constants  $W_{a,b,c}$  with fluctuations along the ( $a, b, c$ ) axes, respectively. The straightforward generalization of  $T_1$  is to  $T_{1z}^{-1} = W_x + W_y$ , where ( $x, y, z$ ) is any permutation of ( $a, b, c$ ). For spin-echo decay the decay process is a single exponential with a decay rate  $T_{1E}^{-1} = 2W_0(I + \frac{1}{2})^2$  for the isotropic case.<sup>33</sup> For the fully anisotropic case the latter formula is straightforwardly generalized to

$$T_{1Ez}^{-1} = (W_x + W_y)[I(I+1) - \frac{1}{4}] + W_z, \quad (\text{A1})$$

where  $T_{1Ez}$  is the echo relaxation time with the field along the  $z$  axis in the same notation. It is also useful to express  $T_{1Ez}$  in terms of  $T_1$  values measured along various axes  $T_{1x,y,z}$ . Equation (A1) then becomes

$$T_{1Ez}^{-1} = T_{1z}^{-1}[I(I+1) - \frac{3}{4}] + \frac{1}{2}[T_{1x}^{-1} + T_{1y}^{-1}]. \quad (\text{A2})$$

In the axial case with  $I = \frac{3}{2}$ , Eq. (A2) becomes  $T_{1Ez}^{-1} = 3T_{1z}^{-1} + T_{1xy}^{-1}$ , where  $T_{1x} = T_{1y} = T_{1xy}$ , as given in Refs. 34 and 35.

For the  $^{17}\text{O}$  echo decay data in Sec. III B 3, we require a generalization of Eq. (A2) to a quantization axis with an arbitrary field orientation given by Euler angles  $(\theta, \phi)$ . Letting that be the  $z'$  axis, with corresponding  $x'$  and  $y'$  axes such that  $x'$  lies in the  $ab$  plane, the associated rate parameters become  $W_{x'} = W_a \sin^2 \phi + W_b \cos^2 \phi$ ,  $W_{y'} = W_a \cos^2 \theta \cos^2 \phi + W_b \cos^2 \theta \sin^2 \phi + W_c \sin^2 \theta$ , and  $W_{z'} = W_a \sin^2 \theta \cos^2 \phi + W_b \sin^2 \theta \sin^2 \phi + W_c \cos^2 \theta$ . We presume that  $T_1$  for  $^{17}\text{O}$  has an anisotropy corresponding to the hyperfine couplings [Eq. (18)]; thus  $W_\alpha = C_\alpha^2 \xi_0$ , as has been found to be the case for YBCO.<sup>15</sup> Then one finds for the direction  $(\theta, \phi)$ ,

$$T_{1Ez'}^{-1} = [C_a^2 + C_b^2 + C_c^2] \xi_0 + \frac{15}{2} \xi_0 [C_a^2 (\cos^2 \theta \cos^2 \phi + \sin^2 \phi) + C_b^2 (\cos^2 \theta \sin^2 \phi + \cos^2 \phi) + C_c^2 \sin^2 \theta], \quad (\text{A3})$$

where  $I = \frac{5}{2}$  for  $^{17}\text{O}$ . Using  $T_{1c} = 57$  ms (Ref. 12) at  $T = 100$  K, and  $C_{a,b,c} = (108, 64, 77)$  kG/(unit spin),<sup>12</sup> Eq. (A3) then gives the general result used in fitting the data of Fig. 8.

- <sup>1</sup> C. H. Pennington and C. P. Slichter, in *Physical Properties of High Temperature Superconductors II*, edited by D. M. Ginsberg (World Scientific, Singapore, 1990).
- <sup>2</sup> R. E. Walstedt and W. W. Warren, Jr., *Science* **248**, 1082 (1990).
- <sup>3</sup> W. W. Warren, Jr., R. E. Walstedt, G. F. Brennert, G. P. Espinosa, and J. P. Remeika, *Phys. Rev. Lett.* **59**, 1860 (1987).
- <sup>4</sup> T. Imai *et al.*, *J. Phys. Soc. Jpn.* **57**, 1771 (1988); **57**, 2280 (1988).
- <sup>5</sup> P. C. Hammel, M. Takigawa, R. H. Heffner, Z. Fisk, and K. C. Ott, *Phys. Rev. Lett.* **63**, 1992 (1989).
- <sup>6</sup> W. W. Warren, Jr. *et al.*, *Phys. Rev. Lett.* **62**, 1193 (1989); R. E. Walstedt *et al.*, *Phys. Rev. B* **41**, 9574 (1990).
- <sup>7</sup> Y. Yoshinari, H. Yasuoka, Y. Ueda, K. Koga, and K. Kosuge, *J. Phys. Soc. Jpn.* **59**, 3698 (1990).
- <sup>8</sup> M. Takigawa *et al.*, *Phys. Rev. B* **43**, 247 (1991).
- <sup>9</sup> E. Oldfield *et al.*, *Phys. Rev. B* **40**, 6832 (1989); L. Reven *et al.*, *ibid.* **43**, 10466 (1991).
- <sup>10</sup> K. Ishida *et al.*, *J. Phys. Soc. Jpn.* **60**, 3516 (1991).
- <sup>11</sup> T. Imai *et al.*, *J. Phys. Soc. Jpn.* **59**, 3846 (1990).
- <sup>12</sup> R. E. Walstedt, B. S. Shastry, and S-W. Cheong, *Phys. Rev. Lett.* **72**, 3610 (1994).
- <sup>13</sup> B. S. Shastry, *Phys. Rev. Lett.* **63**, 1288 (1989).
- <sup>14</sup> N. Bulut, D. W. Hone, D. J. Scalapino, and N. E. Bickers, *Phys. Rev. Lett.* **64**, 2723 (1990); *Phys. Rev. B* **41**, 1797 (1991).
- <sup>15</sup> A. J. Millis, H. Monien, and D. Pines, *Phys. Rev. B* **42**, 167 (1990); A. J. Millis and H. Monien, *ibid.* **45**, 3059 (1992).
- <sup>16</sup> J. Rossat-Mignod *et al.*, *Physica B* **169**, 58 (1991).
- <sup>17</sup> J. M. Tranquada *et al.*, *Phys. Rev. B* **46**, 5561 (1992).
- <sup>18</sup> M. Sato *et al.*, *J. Phys. Soc. Jpn.* **62**, 263 (1993).
- <sup>19</sup> H. A. Mook, M. Yethiraj, G. Aeppli, T. E. Mason, and T. Armstrong, *Phys. Rev. Lett.* **70**, 3490 (1993).
- <sup>20</sup> J. P. Lu, Q. Si, J. H. Kim, and K. Levin, *Phys. Rev. Lett.* **65**, 2466 (1990); *Physica C* **179**, 191 (1991); Q. Si, Y. Zha, K. Levin, and J. P. Lu, *Phys. Rev. B* **47**, 9055 (1993).
- <sup>21</sup> P. B. Littlewood *et al.*, *Phys. Rev. B* **48**, 487 (1993).
- <sup>22</sup> S-W. Cheong *et al.*, *Phys. Rev. Lett.* **67**, 1791 (1991); T. E. Mason, G. Aeppli, and H. Mook, *ibid.* **68**, 1414 (1992).
- <sup>23</sup> G. Aeppli, T. E. Mason, S. M. Hayden, and H. A. Mook

(unpublished).

- <sup>24</sup> M. Matsuda *et al.*, *Phys. Rev. B* **49**, 6958 (1993).
- <sup>25</sup> P. W. Anderson, *Science* **235**, 1196 (1987).
- <sup>26</sup> F. C. Zhang and T. M. Rice, *Phys. Rev. B* **37**, 3759 (1988).
- <sup>27</sup> C. H. Pennington and C. P. Slichter, *Phys. Rev. Lett.* **66**, 381 (1991).
- <sup>28</sup> Y. Itoh *et al.*, *J. Phys. Soc. Jpn.* **61**, 1287 (1992).
- <sup>29</sup> T. Imai, C. P. Slichter, A. P. Paulikas, and B. Veal, *Phys. Rev. B* **47**, 9158 (1993).
- <sup>30</sup> A. Abragam, *The Principles of Nuclear Magnetism* (Oxford University Press, Oxford, 1961).
- <sup>31</sup> C. P. Slichter, *Principles of Magnetic Resonance* (Harper & Row, New York, 1963).
- <sup>32</sup> This form for the rotating-frame spin-spin coupling terms is valid for dipolar coupling and for indirect coupling of the form  $AI_x I'_x + BI_y I'_y + CI_z I'_z$  in the laboratory frame. In the latter case, the resulting secular terms in the rotating frame have the form  $\frac{1}{2}(A+B)\mathbf{I} \cdot \mathbf{I}' + [C - \frac{1}{2}(A+B)]I_z I'_z$ .
- <sup>33</sup> R. E. Walstedt, *Phys. Rev. Lett.* **19**, 146 (1967); **19**, 816 (1967).
- <sup>34</sup> C. H. Pennington *et al.*, *Phys. Rev. B* **39**, 274 (1989).
- <sup>35</sup> T. Imai, C. P. Slichter, K. Yoshimura, M. Katoh, and K. Kosuge, *Phys. Rev. Lett.* **71**, 1254 (1993).
- <sup>36</sup> E. L. Hahn, *Phys. Rev.* **80**, 580 (1950).
- <sup>37</sup> Ref. 1, Chap. XII.
- <sup>38</sup> The like-spin second moment for spin-echo decay is  $\langle \Delta\omega^2 \rangle_A = \frac{1}{8} f_A \sum_j \alpha_{ij}^2$ , where  $f_A$  is the isotopic abundance of  $A$  spins, and  $\frac{1}{8}$  is  $I(I+1)/3$  for a fictitious spin of one-half times  $\frac{1}{2}$  to include only spins which are in the  $\pm \frac{1}{2}$  state.
- <sup>39</sup> A. Narath, *Phys. Rev.* **162**, 320 (1967).
- <sup>40</sup> In order of increasing decay rate, the eigenvectors for Eq. (9) are  $[1,1,1]$ ,  $[3,1,-1,-3]$ ,  $[1,-1,-1,1]$  and  $[1,-3,3,-1]$ .
- <sup>41</sup> We adopt a simplified notation for the  $m$  states,  $[\frac{3}{2}, \frac{1}{2}, -\frac{1}{2}, -\frac{3}{2}] \rightarrow [1,2,3,4]$ , and defining  $f_2 = \exp(-2W_0 t)$ ,  $f_3 = \exp(-6W_0 t)$ ,  $f_4 = \exp(-12W_0 t)$ , we have, for the  $P_{m',m}$ 's,  $P_{1,1} = P_{4,4} = (5 + 9f_2 + f_3 + 5f_4)/20$ ,  $P_{2,2} = P_{3,3} = (5 + f_2 + 9f_3 + 5f_4)/20$ ,  $P_{1,2} = P_{2,1} = P_{3,4} = P_{4,3} = (5 + 3f_2 - 3f_3 - 5f_4)/20$ ,  $P_{1,3} = P_{3,1} = P_{2,4} = P_{4,2} = (5 - 3f_2 + 3f_3 - 5f_4)/20$ ,  $P_{1,4} = P_{4,1} = (5 - 9f_2 - f_3 + 5f_4)/20$ ,  $P_{2,3} = P_{3,2} = (5 - f_2 - 9f_3 + 5f_4)/20$ .

- <sup>42</sup> One can use here, for example, the motional narrowing formula from Ref. 1, Chap. X:  $T_2^{-1} = \langle \Delta\omega^2 \rangle \int_0^\infty g(\tau) d\tau$ , where  $g(\tau)$  is the correlation function of the interaction which contributes the second moment  $\langle \Delta\omega^2 \rangle$ .
- <sup>43</sup> In generating these decay curves it became quite evident that the long-time decay function is quite sensitive to fine details about the distribution of interaction strengths employed. It was necessary to average results from several sets of random couplings to obtain smooth curves.
- <sup>44</sup> K. Yoshinara *et al.*, J. Phys. Soc. Jpn. **58**, 3057 (1989).
- <sup>45</sup> M. A. Kennard, Y.-Q. Song, K. R. Poeppelmeier, and W. P. Halperin, Chem. Mater. **3**, 672 (1991).
- <sup>46</sup> D. E. Farrell *et al.*, Phys. Rev. B **36**, 4025 (1987).
- <sup>47</sup> F. Mila and T. M. Rice, Physica C **157**, 561 (1989).
- <sup>48</sup> We make estimates of the Cu hyperfine constants  $A_{ab}$ ,  $A_c$ , and  $B$  using data from the literature. The coincidence of  $T_1$  curves for doped and undoped LSCO at high temperatures (Ref. 50) suggests similar transverse hyperfine parameters for these systems. Thus, we assume the value  $A_{ab} - 4B = -139g_{ab} = -286$  kG/spin from the undoped case (Ref. 50), where we take  $g_{ab} = 2.06$  (Ref. 12). For  $A_c$  we compare shift (Ref. 51) and susceptibility (Refs. 10,12) results to find  $dK_c^s/d\chi_c^s = 1.0$  (emu/mol)<sup>-1</sup>. This, in turn, gives  $A_c + 4B \approx 13$  kG/spin. Finally, estimating  $K_{ab}^s = 0.35\%$  from Ref. 51 and taking  $\chi_{ab}^s = 146 \times 10^{-6}$  (emu/mol) (Ref. 12), we obtain  $A_{ab} + 4B \approx 294$  kG/spin. This number may vary if portions of  $K_{ab}^s$  and  $\chi_{ab}^s$  are allocated to a second band in accord with the findings of this paper and Ref. 12. Using  $A_{ab} + 4B = 294$  kG/spin, one finds  $A_{ab} = 4$ ,  $A_c = -277$ , and  $B = 72.5$ , all in kG/spin.
- <sup>49</sup> Orientation of the LSCO crystal with respect to the  $\mathbf{q}$  is unspecified in Ref. 23. We shall interpret data given for  $\chi_0''(\omega, T)$  as a powder average. This is expected to be correct to better than 10%. The orientation dependence of  $\chi_\alpha(r_{ij})$  [Eq. (14)] is taken to be  $\chi_\alpha(r_{ij}) \propto g_\alpha^2$ , where  $g_{ab,c} = (2.06, 2.27)$  (see Ref. 12).
- <sup>50</sup> T. Imai, C.P. Slichter, K. Yoshimura, and K. Kosuge, Phys. Rev. Lett. **70**, 1002 (1993).
- <sup>51</sup> T. Imai, Ph.D. thesis, The University of Tokyo, 1991.
- <sup>52</sup> At large exchange frequencies, the effect of the  $m = \pm\frac{1}{2}$  fluctuations on the echo decay weakens, and these levels merge into an effectively  $m = 0$  level. However, the  $T_1$  fluctuations between the  $\pm\frac{3}{2}$  levels and the effective  $m = 0$  level now take on a larger amplitude, compensating for the loss of the  $\pm\frac{1}{2}$  level contribution. The contrast between <sup>63</sup>Cu and <sup>65</sup>Cu effects in Fig. 7(b) apparently depends on subtle differences between like-spin and unlike-spin relaxation terms.
- <sup>53</sup> H. Monien, P. Monthoux, and D. Pines, Phys. Rev. B **43**, 275 (1991).
- <sup>54</sup> F. Mila, Phys. Rev. B **42**, 2677 (1992).
- <sup>55</sup> A. J. Millis and H. Monien, Phys. Rev. Lett. **70**, 2810 (1993).
- <sup>56</sup> T. Imai *et al.*, J. Phys. Soc. Jpn. **59**, 3846 (1990).
- <sup>57</sup> V. Barzykin, D. Pines, and D. Thelen (unpublished).